Anexo A

A METHOD TO IMPROVE THE ACCURACY OF CONTINOUS MEASURING OF VERTICAL PROFILES OF TEMPERATURE AND WATER VAPOR DENSITY BY MEANS OF A GROUND-BASED MICROWAVE RADIOMETER

Sánchez, J. L.[a,*], Posada, R.[a], García-Ortega, E.[a], López, L.[a], Marcos, J. L[a]

[a] *University of León, Spain*

Abstract

Many of the meteorological phenomena occurring at meso-γ require observations sufficiently close together in time and space. The multichannel microwave radiometer (MMWR) provides continuous temperature and humidity profiles. We demonstrate a method for profile bias correction that significantly improves vertical temperature (T) and water vapor density (δ_{wv}) profile accuracy. We compared MMWR temperature (T_{RD}) and humidity ($\delta_{wv_{RD}}$) profiles during winter in the Sierra of Guadarrama (Madrid) at 1150 m altitude with thousands of radiosonde temperature (T_{RW}) and humidity ($\delta_{wv_{RW}}$) soundings from a launch site at 610 m altitude and 50 km distance. In spite of relatively large horizontal and vertical separation between the two sites, sounding differences above the boundary layer are comparable to observation error typically assigned to radiosonde soundings when they are assimilated into numerical weather models. Systematic bias between the paired values of T_{RW} and T_{RD} and $\delta_{wv_{RW}}$ and $\delta_{wv_{RD}}$ ranges from 0.2 to 1.2 K and 0.05 to 0.5 g m^{-3}. This bias can be removed using a corrector function that is applied at each T and δ_{wv} level. Using this method, the bias for both variables is reduced to insignificant levels and their accuracy is significantly improved.

*Corresponding author: Group for Atmospheric Physics, Instituto de Medio Ambiente
Email address: jl.sanchez@unileon.es (Sánchez, J. L.)

Keywords: ground-based microwave radiometer; temperature and humidity profiles; continuous measuring; radiosonde sounding

1. Introduction

Atmospheric movements occur over a broad continuum of space and time scales: from seconds to days and from microns to thousands of kilometers. Terrain height variations and differential surface fluxes of heat momentum and moisture affect meteorological phenomena on a wide range of scales. Many of them occur at meso-γ as a result of topographic forcing-and a combination of a variety of instability operating on this scale. Consequently, those phenomena and the intensity to which they occur can be featured by observations sufficiently close together in time and space and, therefore, we can determine the mesoscale factors on which they depend. However, the lack of observations necessary to define mesoscale systems is a critical meteorological problem.

In order to settle this difficulty, one option is to use numerical models complemented with sensibility analysis, since it allows us to study the mesoscale factors that intervene in the appearance of a meteorological perturbation, and estimate the influence of each one of these factors (for instance, García-Ortega et al., 2007, 2009, Vich et al., 2011). However, the formulation of the models contains nonlinear equations of motion and continuity equations for mass heat and water, which can only be solved with approximations. At the same time, the resolution of these equations requires to know, for a given boundary, the initial meteorological conditions. Again, we find ourselves with a situation in which the predictability of a model depends on the initial conditions being established with the greatest detail and precision possible. In other words, there are factors that intervene, such as the density of meteorological observation stations on the surface, and the number of weather balloons that can be used, among others. However, the number of rawinsonde launching stations included in the worldwide network is sparse and generates data only twice per day.

In order to establish the initial conditions for a mesoscale model, we need to perform a series of steps (Sashegyi and Madala, 1994), including: (i) quality con-

trol, (ii) objective analysis and (iii) initialization and assimilation. Both in the first and in the last step, the observed data intervenes in a decisive way. Here we see that, in addition to being sparse, there tend to be errors and/or data gaps (Soden and Lanzante, 1996, Schwartz and Doswell, 1991). Furthermore, there are two additional aspects that have to be monitored in regard to meteorological observation and the treatment of databases: the registers have to be done with “adequate” frequency, and a ”good“ method must be chosen to assimilate the data. With all of this, we obtain, as accurately as possible, the state of the atmospheric flow on a regular grid. If we pay attention to these two aspects, the characterization of the initial conditions will be reasonably predicted. But, a small error in the initial conditions affects the results of the numerical models, and as such, this affects the quality of the forecast in terms of space and time. This is especially relevant for many meteorological phenomena, and especially for those related to the precipitation processes.

From all of the above, we can establish that the capacity to make forecasts using Numerical Weather Predictions (NWPs) depends, in large part, on the quality and frequency of data observed. Introducing the time dimension in the assimilation period guarantees a better treatment of the data, which is not centered solely on the main synoptic time (Rabier, 2005). For instance, when we try to improve the quality of the predicted precipitation field, one option is to use the observations made by satellites and incorporate them into the initialization process. We have a few examples, such as in the BOLAM model (Lanciani et al., 2008, Davolio and Buzzi, 2004), which employs a data-assimilation scheme that takes into account the precipitation field estimated by satellites. The results allow us to improve forecasts, even in the case of flooding conditions (Malguzzi et al., 2006). Other authors (Michaelides et al., 2009), point out that the non-linear 4D-Var assimilation methods from geostationary satellite observations improve the models' forecasting.

It seems reasonable to assume that the use of high-frequency sampling of thermodynamic profiles allows for a better understanding of some mesoscale phenomena, since they improve the predictability of the NWPs. The sparce network of rawinsonde launching stations, made it necessary to turn to different alternatives. For instance, we can make use of polar orbiting satellites since they are capable of

estimating vertical profiles of temperature and moisture. They have an advantage since satellites have global coverage, but the accuracy and the vertical resolution at lower levels are limited (Zhou et al., 2007).

If knowing the vertical profiles of temperature in the greatest number of observation points is important, along with it being done at a good frequency, the case of the water vapor measurement is even more important due to its variability in terms of space and time. In many processes, for example, cloud formation and precipitation, the role that water vapor plays is very important. Some Projects, such as WALES (ESA, 2003) have allowed us to know the possibilities that represent the different water vapor measurement systems taken from space. So, Wulfmeyer et al. (2005) did a comparative analysis of active and passive water vapor remote sensing from space by means of lidar technology. In the Global Water Vapor Project of WMO (Randel et al., 2011), a combination of rawinsondes and passive remote sensing systems were used to derive blended global water vapor data sets for climate research. In general, the difficulty involved in adequately measuring water vapor in the atmosphere provokes limitations in the initialization of numerical models, and, as a consequence, the quality of precipitation and cloud-formation forecasting is affected (Hagemann et al., 2004).

At this point, it seems necessary to turn to methods other than rawinsondes. There are basically two options: ground-based microwave radiometric profilers and Fourier transform infrared emission spectroscopy (FTIR) (Knuteson et al., 2004a, 2004b). The former are very sensitive to precipitation, while the latter are impeded in cloudy fields of vision and are restricted to the subcloud layer (and, as such, they are used in studies orientated toward atmospheric contamination (Feltz at al., 1998, Spänkuch at al., 1996, 1998, 2000) in the boundary layer. Multichannel ground-based microwave radiometers (MMWR) can be used as profilers of temperature and humidity since they allow us, unlike with traditional rawinsondes, to obtain constant continuous measurements of water vapour profiles and estimated integrated water vapor (IWV). They have the advantage of high-frequency sampling of thermodynamic profiles, with a resolution at levels between 50 and 250 m, and can reach a height of up to 10,000 meters. MMWR profiling methods make use of atmospheric radiation measurement in the range of 20 to 200 GHz.

MMWRs have been used in different projects. For example, in the Baltex Bridge Campaign, CLIMA-NET and ARM (Cimini et al., 2011, Cimini et al., 2006, Friedrich et al., 2012, Spänkuch et al., 2011, Löhnert and Maier, 2012, Crewell et al., 2004, Güldner and Leps, 2005, Turner et al., 2003, Mattioli et al., 2007), the results show the advantages of continuous measurements of water vapor and its influence in cloud formation. Güldner and Spänkuch, 2001, investigated the capacity of MMWRs to sound the thermodynamic state of the atmosphere almost continuously, and found an accuracy of the retrieved temperature profiles from 0,6 K near the surface to 1,6 K at 7 km. In the case of water vapour density, the accuracy of profiles was 0,2-0,3 g m^{-3} near the surface to 0.8-1.0 g m^{-3} at an altitude of 2 km. Recently, Knupp et al. (2009) did an analysis of the capacity of a ground-based passive profiling of MMRW to characterize the atmosphere in different dynamic weather conditions. They selected a series of meteorological events and, using MMWR, analyzed the continuous thermodynamic profiles of temperature and moisture. Iassamen et al., 2009 analyzed, via MMRW, the distribution of tropospheric water vapor in clear and cloudy conditions, finding a close relationship to those found by the European reanalysis meteorological database ERA 15. Similarly, radiometric retrievals compare fairly well with the corresponding values obtained from the operational rawinsonde dataset.

Within the context of TECOAGUA Project, a series of measurements that are conducive to both characterizing the winter precipitation processes that affect the Central Mountain Range of the Iberian Peninsula, and to improving the predictability of snowfall in Madrid, were carried out. In this paper, we will focus on the comparison of the data of thermodynamic profiles using MMWR obtained during three winter seasons with those provided by the rawinsonde station in Madrid-Barajas Airport. All of this is done with the objective of knowing the accuracy of MMWR measurements and to be able to introduce data assimilation techniques to the initialization of mesoscale models.

2. Radiometer and noise

The MMWR used is an MP-3000A Hyper-Spectral Microwave Radiometer (manufactured by Radiometrics). Profiles are retrieved from a subset of 35 chan-

nels (21 K-Band and 14 V-Band), by means of the Stuttgart Neural Network Simulator (SNNS) trained with 10 years of historical soundings from 3 rawinsonde stations. Profiles of temperature (T), and water vapor density (δ_{wv}) are obtained approximately every 2.5 minutes.

Ten years of RAOBs from Madrid-Barajas and Coruña (both in Spain) and Denver (USA) were used as the training set of a neural network. Denver was chosen because it is located at a latitude and altitude similar to the placement of the MMWR (N 41^{o} W 4^{o}, 1110 MSL), and there is no other similar station in the Iberian Peninsula. The MMWR was placed in the Central Mountain Range, (see Figure 1) at a height of 1150 MSL, about 70 km to the north of Madrid and 50 km from the rawinsonde station at Madrid-Barajas (situated at 610 MSL). The neural network retrievals were based on all-season retrievals, although in this paper, we only refer to those retrieved in the winter periods of 2009-10 and 2010-11 since some of the data obtained by the MMWR were used to support part of the TECOAGUA Project (whose objectives were focused on the analysis of winter cloud masses which produce snow precipitation in the Central Mountain Range).

Once the MMWR was placed on the field, we tested the LWP (liquid water path) values on 52 completely cloudless days, since the expected value would be 0 mm. With a total of 54,325 profiles retrieved by the MMWR in these conditions, we obtained an average LWP of 0.021 mm, which led us to establish that the background noise is very low both during the day and at night.

Some authors, such as Hewison (2007), have established the threshold value of LWP in conditions of completely cloudless skies at a value of 0.017 mm, which is in accordance with our results. Therefore, we concluded that the power receiver of our MMWR has a highly stable noise-diode as a gain reference.

3. Data stratification

The initial objective was to determine the validity of T and δ_{wv} retrievals for each of the levels/profiles obtained via the MMWR. We had to consider that the retrievals can be affected by liquid precipitation, which can alter the measurement of the signal received. Some authors use this fact, along with data obtained from

MMWRs, to make an estimate of rain (Marzano et al., 2002, 2006).

The MMWR that we used has a precipitation sensor that marks Yes/No for precipitation, but in our case, we decided to complement it with a Visibility and Present Weather sensor (VPF-730) that, along with presenting less uncertainty than the MMWR sensor, it also classifies types of precipitated hydrometeors. Thus, for each profile we can identify if it was affected by precipitation and if it was liquid or snow.

To continue on to the comparison between the MMWR and the rawinsonde at Madrid-Barajas at 0000 and 1200 UTC, we took the retrievals from the MMWR between 2330 UTC to 0030 UTC, and we calculated the average values in order to obtain mean temperature and water vapor profiles at 0000 UTC. Similarly, we obtained data at 1200 UTC, taking the mean profile of the retrievals from 1130 UTC to 1230 UTC. Despite the fact that the precipitations have been mostly in snow form, the data sample was stratified into three different groups, according to the following criteria:

- Group 1: All of the vertical profiles for T and δ_{wv} at 0000 and 1200 UTC independent of whether precipitation was registered over the MMWR. The sample size (N) used was of 18304 profiles.
- Group 2: Extracting the vertical profiles obtained while precipitation was absent from Group 1. The sample size (N) was of 6226 profiles.
- Group 3: Extracting the profiles obtained while precipitation was registered over the MMWR from Group 1. The sample size (N) was of 2645 profiles.

It is necessary to consider that the neural network retrieval outputs give 58 levels from the ground to 10 km AGL. The vertical resolution for the MMWR is 50 m near the surface to about 500 m, 100 m to about 2 km and 250 m to about 10 km. Consequently, the radiometer retrieval accuracy is higher near the surface and decreases with height. Thus, on one hand, we took the values obtained at each level for T and δ_{wv}, and, on the other hand, the same variables obtained with the corresponding RAOB sounding at the Madrid-Barajas station. In doing this, we were able to establish a correlation between estimated temperature from the

MMWR and the observed T from RAOB at each level (i) (which will be named from now on as T_{RD_i} and T_{RW_i} , respectively). Analogously, we could establish a correlation between the estimated density of water vapor from MMWR and the observed density from RAOB from Madrid-Barajas (named $\delta_{wv_{RD_i}}$ and $\delta_{wv_{RW_i}}$, respectively).

4. Results of the comparison between radiosounding vs. MMWR profiles

The results obtained from the comparison of T, for the three groups are shown in Figures 2 to 4. Figures 5 to 7 show the comparison of δ_{wv} for the same three groups. As can be seen, the correlation coefficients of T are of the order of 0.99 for the three groups. The slopes are about 0.98. For δ_{wv}, the correlation coefficients take values of 0.94, 0.90 and 0.96 for each of the three groups, respectively, and slopes are 0.94, 0.91 and 1.00, respectively, for the groups. In other words, the fit is slightly worse in situations with no precipitation. Although in general, the MMWR and RAOB data from Madrid-Barajas fit well, we can see that in situations with precipitation and with greater water vapor concentration, the fit is better. Thus, we can conclude that there are barely any differences between the different groups. This result was expected, considering that in most of the occasions with precipitation, it was in snow form and this affects neither the K-Band nor the V-Band frequencies in which MMWR operates (Kneifel et al. 2010). So, we can use the entire winter data sample independent of whether or not there is winter precipitation.

Considering the importance that small variations of T and δ_{wv} have in the initialization of the mesoscale models, we have calculated the bias and the root mean square (rms), along with the standard deviation. In Figures 8 to 10, we see the results for each of the groups, both for T and δ_{wv}. In all three cases, the behavior was similar. So, the temperature in the level closest to the ground shows an rms that is somewhat greater than at the other levels (which is attributable to the environmental conditions at the boundary layer, which are different from the location of the MMWR and the rawinsonde at Madrid-Barajas). Above this layer, the temperature presents an rms between 1.5 K and 3 K, except at the levels superior to 10 km, which reach about 4 K. Thus, the lowest rms values are found at levels below

2.8 km MSL. It seems clear that above 9 km MSL, the retrievals obtained by the MMWR separate from the RAOB measurements at Madrid-Barajas. In the case of the biases, they are, on average, close to 0, with a tendency to be negative until the first 5 km MSL. The biggest difference is registered at a height of about 3 km, and, as we can see, the retrievals tend to underestimate the value of temperature until 6 or 7 km MSL. Beyond that point, the retrievals begin to overestimate temperature. In the analysis of the standard deviations we can see that the variability is greater in the profiles of the RAOB than for the MMWR, which seems to mean that the RAOBs used are more sensitive to the changes in the values of the variables.

Upon analysing the results of water vapor density (Figures 8 to 10), the rms values obtained are very satisfactory since at the lower levels, they are below 1 g m^{-3} in the three groups, and the biases are close to 0 at every level, being somewhat worse in the lower levels than in the higher ones.

As such, in the previous analysis, we can say that the retrievals of the T and δ_{wv} profiles obtained by the MMWR for the winter campaigns are consistent with data from the RAOB at Madrid-Barajas. The fact that there was a discrepancy in the levels closest to the ground is due to the fact that they are located in different places and at different heights. Above this level, the rms shows relatively stable values, around 2.5 K. Thus, the reconstruction of the temperature and water vapor profiles for our MMWR can be considered satisfactory and are better than those found by Güldner and Spänkuch (2001) and Liljegren et al. (2001), when they compared these same variables obtained with an MMWR similar to ours with data provided by the RAOB of a nearby rawinsonde station. It is useful to point out that typical observation error assigned to radiosonde soundings when they are assimilated into models vary between 1.3 and 2.2 ^{o}C for temperature and 1.6 and 2.4 g m^{-3} for humidity (Cimini et al., 2011, Knupp et al., 2009).

5. A method to diminish uncertainty: correcting the profiles layer by layer

Although the values for T and δ_{wv} retrieved by the MMWR are acceptable, it is clear that we should try to diminish uncertainty. Keeping the importance of these variables in mind, the existence of these discrepancies among the RAOB data

from Madrid-Barajas and the MMWR, have motivated us to look for a correction method that will simplify and improve systematically the reconstructions of the atmospheric profiles. The special feature of this method is that it does not correct the profile in its entirety; rather, it does so layer by layer. In doing so, at each layer, a correction factor is calculated. The final objective is to reduce the discrepancy between the T_{RD_i} and T_{RW_i} profiles, and between the $\delta_{wv_{RD_i}}$ and $\delta_{wv_{RW_i}}$ profiles estimated by the MMWR and RAOB sounding, respectively. Thus, we can reduce the retrievals' uncertainties for the T and δ_{wv} and use them operatively at heights greater than those proposed by other authors (at heights of 3 to 5 km, e.g. Güldner and Spänkuch, 2001; Hewison, 2007).

This method is based on a linear regression, in which the correction factors are calculated for each of the 58 layers. To do this, we used the following methodology:

- First, the initial sample of 338 days was divided into two random sub-samples: the first one (Sub-sample 1) contains 66.6% of the total days (225 days), and was used to find the best possible fits (level by level). The second one (Sub-sample 2) contains the remaining 33.4 % (113 days), and it was used to validate the model-fitting.

- For each layer,i, and for Sub-samples 1 and 2, databases were constructed obtaining the paired values for T_{RD_i} and T_{RW_i}, and $\delta_{wv_{RD_i}}$ and $\delta_{wv_{RW_i}}$ respectively, according to the method described in the previous section. The paired values from Sub-sample 1 were compared layer by layer, so that we obtained a correction factor for each variable and for each layer. Figure 11 (left) shows the rms values obtained after comparing T_{RD_i} and T_{RW_i} of Sub-sample 1 before (rms_1) and after applying the model-fitting ($rms_1{}'$). It can be seen that the values were close to 2 K up to 3000 MSL and they exceed 3 K upwards of 9000 MSL. The $rms_1{}'$ manifests lower values, especially at high heights. In Figure 11 (right), rms_1 is presented for water vapour density. Although the uncertainty of the measurement can seem like a very low value, an rms of 1 g m^{-3} at low levels usually represents situations of precipitation to the order of 20-25% of water vapor density in the area in winter.

- Afterwards, we took Sub-sample 2 with the paired TRD2i and TRW2i, and $\delta_{wv_{RD2_i}}$ and $\delta_{wv_{RW2_i}}$ data, respectively, and applied the model-fitting to a stretch of data, following the methodology mentioned in the previous point. In this way, with the second sub- sample, we can validate the fit and discuss the results.

In order to validate the model-fitting, we applied the correction factors obtained from Sub-sample 1 to the T_{RD_i} and $\delta_{wv_{RD_i}}$ of Sub-sample 2. Figure 12 (left) shows the rms of temperature before (rms_2) and after ($rms_2{}'$) the correction factors were applied. As a result, the uncertainty of T diminished, since the error was reduced at every level, and especially at higher altitudes, where $rms_2{}'$ decreased more than 1 K. The correction factors applied to the $\delta_{wv_{RD_i}}$ in Sub-sample 2 also improved the retrievals of water vapor density. The $rms_2{}'$ values are 0.2 g m^{-3} inferior to the rms of Sub-sample 2 (rms_2) at levels up to 4500 MSL, as we can see in Figure 12 (right).

6. Discussion and conclusions

Continuous measurements done using MMWR can be very useful for the detection of mesoscale phenomena that require very high spatial and temporal scales. However, this measurement technology is based on an indirect measurement and, as such, it is necessary to know the uncertainty of these measurements. In our case, vertical profiles were initially retrieved from a subset of 35 channels by means of the Stuttgart Neural Network Simulator trained with 10 years of historical soundings from 3 rawinsonde stations.

In comparing data for temperature and water vapor density obtained by the MMWR and from the rawinsonde station at Madrid-Barajas, we were able to prove that there is a good correlation between both stations, with correlation coefficients superior to 0.90 in the case of water vapor, and 0.99 for temperature. Since the measurement campaigns were carried out in winter conditions and in a mountainous area, the precipitation in snow form did not affect the measurements. When T and δ_{wv} vertical profiles were analyzed layer by layer, we were able to prove that while some strati adjusted quite well (there are barely differences between the RAOB and MMWR data), in other cases, some biases were detectable, and some rms values were not very satisfactory.

Using a linear adjustment method, stratus by stratus, it was possible to limit the discrepancy to be no greater than 1K at all heights, and in the case of water vapor density, it did not exceed 0.2 g m^{-3}.

In these conditions, the method allows us to diminish the characterization of the initial conditions that can be done using continuous MMWR measurements. With these values, we believe we have objective criteria that can be applied to improve T and δ_{wv} retrievals. In turn, they can be used as data assimilation for improving the forecasting of mesoscale phenomena with NWP models.

Acknowledgments

This paper was done supported by the following grants: Micrometeo.com (IPT-310000-2010-22) and Granimetro Projects (CGL2010-15930). Special thanks for

Estibaliz Gascón, Santiago Gómez, Roberto Weigand and Lauren Giera. We would like to thank the Canal de Isabel II for the facilities used to install the MMWR.

References

[1] Cimini D., E. Campos, R. Ware, S. Albers, G. Giuliani, J. Oreamuno, P Joe, S. E. Koch, S. Cober, and E. Westwater, 2011. Thermodinamic Atmospheric Profiling During the 2010 Winter Olimpic Using Ground-Based Microwave Radiometry. IEEE Trans. Geosci. Remote Sens. Doi:10.1109/TGRS.2011.154337.

[2] Cimini D., T. Hewison, L. Martin, J. Güldner, C. Gaffard and F. Marzano. 2006. Temperature and humidity profile retrievals from ground-based microwave radiometers during UTC. Meteorolo. Z. 15, 45-56 doi:10.1127/0941-2948/2006/0009.

[3] Davolio S., A. Buzzi, 2004. A nudging scheme for the assimilation of precipitation data into a mesoscale model. Wea. Forecasting, 19, 855-871.

[4] ESA 2003. System requirements document for the WALES water vapor lidar experiment in space The five candidate earth explorer core missions. European Space Agency EEM-FP/2001- 12-560.

[5] Feltz, W. F., W. L. Smith, H.B. Howell, R.O. Knuteson, H. Woolf, H. E. Revercomb, 2003. Near- continous profiling of temperature, moisture and atmospheric stability using the Atmospheric Emitted Radiance Interferometer (AERI). J. Appl. Meteor., 42, 584-597.

[6] Friedrich K, J. K. Lundquist, M. Aitken, E Kalina and R. F. Marshall, 2012. Stability and turbulence in the atmospheric layer: A comparison of remote sensing and tower observations. Geophys. Res. Lett., 39, L03801 doi:10.1029/2011GRL050413

[7] García-Ortega, E., L. López, J.L. Sánchez. 2009. Diagnosis and sensitivity study of two severe storm events in the Southeastern Andes. Atmos. Res. 93, 1-3,161-178.

[8] García-Ortega, E., L. Fita, R. Romero, L. López, C. Ramis, J.L. Sánchez. 2007. Numerical simulation and sensitivity study of a severe hailstorm in northeast Spain. Atmos. Res. 83, 2-4, 225-241.

[9] Güldner, J., D. Spänkuch, 2001. Remote Sensing of the Thermodynamic State of the Atmospheric Boundary Layer by Ground-Based Microwave Radiometry. J. Atmos. Oceanic Technol. 18, 925-933.

[10] Hewison, T. J., 2007: Profiling temperature and humidity by ground-based microwave radiometers. PhD Thesis, Department of Meteorology, University of Reading, UK, 191 pp.

[11] Iassamen, A., H. Sauvageot, N. Jeannin, S. Ameur, 2009. Distribution of tropospheric water vapor in clear and cloudy conditions from microwave radiometric profiling. Journal of Applied Meteorology and Climatology. 48 (3), pp. 600-615.

[12] Kneifel S. U. Löhnert, A. Battaglia, S. Crewell, D. Siebler, 2010. Snow scattering signals in ground-based passive microwave radiometer measurements. J. Geophys. Res., 115, D16214, doi:10.1029/2010JD013856, 2010.

[13] Knuteson, R.O., H.E. Revercomb, F.A. Best, N.C. Ciganovich, R.G. Dedecker, T.P. Dirkx, S.C. Ellington, W.F. Feltz, R.K. Garcia, H.B. Howell, W.L. Smith, J.F. Short, D.C. Tobin, 2004. Atmospheric Emitted Radiance Interferometer. Part I: Instrument Design. Journal of Atmospheric and Oceanic Technology. 21, 1763-1776.

[14] Knuteson, R.O. , H.E. Revercomb, F.A. Best, N.C. Ciganovich, R.G. Dedecker, T.P. Dirkx, S.C. Ellington, W.F. Feltz, R.K. Garcia, H.B. Howell, W.L. Smith, J.F. Short, D.C. Tobin. 2004. Atmospheric Emitted Radiance Interferometer. Part II: Instrument Performance. Journal of Atmospheric and Oceanic Technology. 21, 1777-1789.

[15] Knupp, K.R., R. Ware, D. Cimini, F. Vandenberghe, J. Vivekanandan, E. Westwater, T. Coleman, D. Phillips, 2009. Ground-based passive microwave profiling during dynamic weather conditions. Journal of Atmospheric and Oceanic Technology, 26 (6), pp. 1057-1073.

[16] Lanciani A., S. Mariani, M. Casaioli, C. Accadia, N. Tartaglione, 2008: A multiscale approach for precipitation verification applied to the FORALPS case studies. Adv. Geosci., 16, 3-9.

[17] Liljegren, J. C., B. M. Lesht, S. Kato, E. E. Clothiaux, F. S. Solheim,R. H. Ware, 2001. Initial evaluation of profiles of temperature, water vapor and cloud liquid water from a new microwave radiometer. Paper presented at the To Appear in the Preprint Volume of the 11th Symposium on Meteorological Observations and Instruments, Albuquerque, NM.

[18] Löhnert, U. and O. Maier. 2012. Operational profiling of temperature using ground-based microwave radiometry at Payerne: prospects and challenges. Atmos. Meas. Tech, 5, 1121- 1134 doi:10.5194/amt-5-1121-2012.

[19] Malguzzi P., G. Grossi, A. Buzzi, R. Ranzi, R. Buizza, 2006. The 1996 - century- flood in Italy. A meteorological and hydrological revisitation. J. Geophys. Res., 111: D24106.

[20] Marzano F. S, E. Fionda, P. Ciotti, A. Martellucci. 2002. Ground-Based Multifrequency Microwave Radiometry for Rainfall Remote Sensing. IEEE Transactions on Geoscience and Remote Sensing, 40, 4, 742-759.

[21] Marzano F. S.n E. Fionda, P. Ciotti. 2006. Neural-network approach to ground-based passive microwave estimation of precipitation intensity and extinction. J. Hydrology 38, 121-131.

[22] Mattioli, V., E.R. Westwater , D. Cimini, J.C. Liljegren, B.M. Lesht, S.I. Gutman, F.J. Schmidlin, 2007. Analysis of rawinsonde and ground-based remotely sensed PWV data from the 2004 North Slope of Alaska Arctic Winter Radiometric Experiment. Journal of Atmospheric and Oceanic Technology. 24, 3, 415-431.

[23] Michaelides, S., V. Levizzani, E. Anagnostou, P. Bauer, T. Kasparis, J.E. Lane. 2009. Precipitation: Measurement, remote sensing, climatology and modelling. Atmos. Res., 94, 4, 512-533.

[24] Rabier, F., 2005. Overview of global data assimilation developmments in numeriocal weather- prediction centres. Q.J.R. Meteorol., 131, 3215-3233.

[25] Randel, L., C.D. Kummerow, S. Ringerud, J. Crook, D. Randel, W.Berg. 2011. An observationally generated a priori database for microwave rainfall retrievals. Journal of Atmospheric and Oceanic Technology, 28, 2, 113-130.

[26] Sashegyi, K., R. V. Madala, 1994. Initial conditions and boundary conditions. Mesoscale Modelling of the Atmosphere. Meteorological Monographs. AMS. Boston. Vol 25. No. 47. 1- 12.

[27] Schwartz R. S. and C. A. Doswell III. 1991. North American rawinsonde observations: Problems, concerns, and a call to action. Bull. Amer. Meteor. Soc., 72, 1885-1896.

[28] Soden B. J. and J. R. Lanzante. 1996. An assessment of satellite and rawinsonde climatologies of upper-tropospheric water. Journal of Climate, 9, 1235-1250.

[29] Spänkuch, D., W. Döhler, J. Güldner, A. Keens, 1996. Ground-based passive atmospheric remote sounding by FTIR emission spectroscopy-First results with EISAR. Contrib. Atmos. Phys., 69, 97-111.

[30] Spänkuch, D., W. Döhler, J. Güldner, E. Schulz, 1998. Estimation of the amount of tropospheric ozone in a cloudy sky by ground-based Fourier transform infrared emission spectroscopy. Appl. Opt., 37, 3133-3142.

[31] Spänkuch, D., W. Döhler, J. Güldner, 2000. Effect of coarse biogenic aerosol on downwelling infrared flux at the surface. J. Geophys. Res., 105 (D13), 17 341-17 350.

[32] Spänkuch, D., J. Güldner, H. Steinhagen and M. Bender, 2011. Analysis of a dryline-like featured in northern Germany detected by a ground-based microwave profiling Meteorol. Z. 20, 4, 409-421.

[33] Turner, D.D., B.M. Lesht, S.A. Clough, J.C. Liljegren, H.E. Revercomb, D.C. Tobin, 2003. Dry bias and variability in Vaisala RS80-H rawinsondes: The ARM experience. Journal of Atmospheric and Oceanic Technology, 20, 117-132.

[34] Vich, M., R. Romero, H.E. Brooks. 2011. Ensemble prediction of Mediterranean high-impact events using potential vorticity perturbations. Part I: Comparison against the multiphysics approach. Atmos. Res., 102, 1-2, 227-241.

[35] Wulfmeyer V., H. Bauer, P. di Girolamo, C. Serio. 2005. Comparison of active and passive water vapor remote sensing from space: an analysis based on the simulated performance of IASI and space borne differential absorption lidar. Remote Sensing of Environment. 95, 211- 230.

[36] Zhou, D. K., W. L. Smith, X. Liu, A. M. Larar, S. A. Mango and H. L. Huang, 2007. Physically retrieving cloud and thermodynamic parameters from ultraspectral IR measurement. J. Atmos. Sci., 64, 969-982.

List of Figures

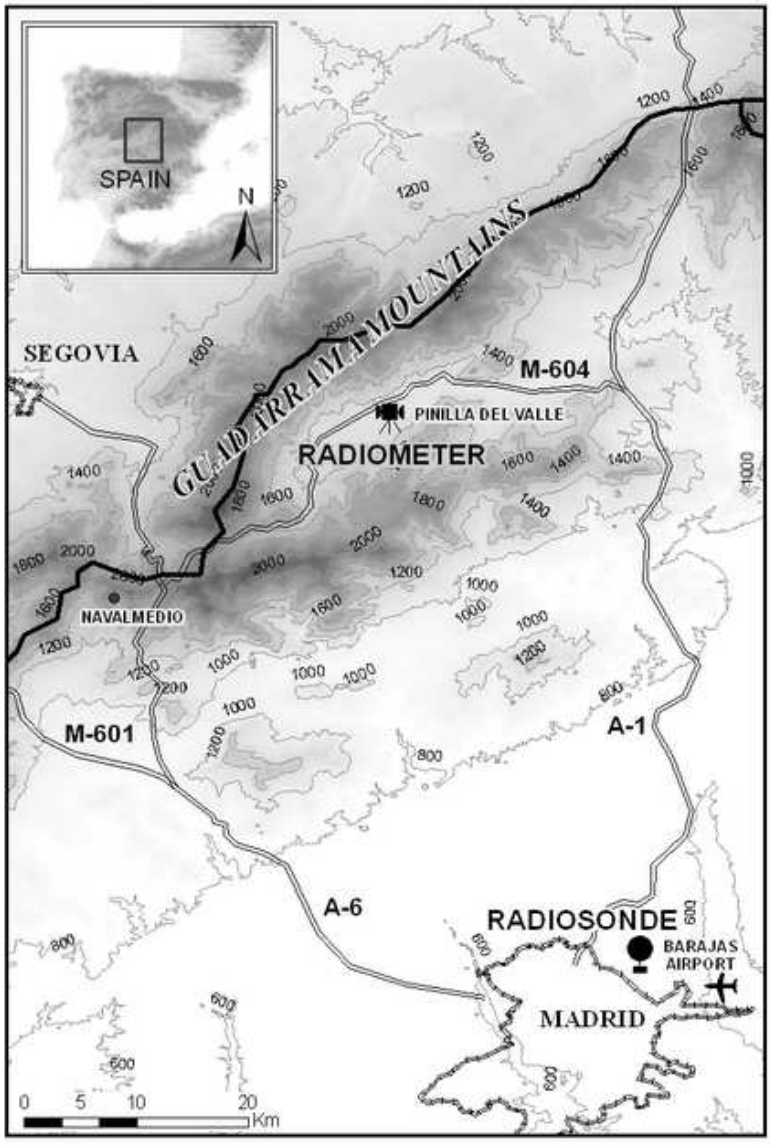

Figure 1: Guadarrama Mountains, Madrid, Barajas Airport and the Radiometer position.

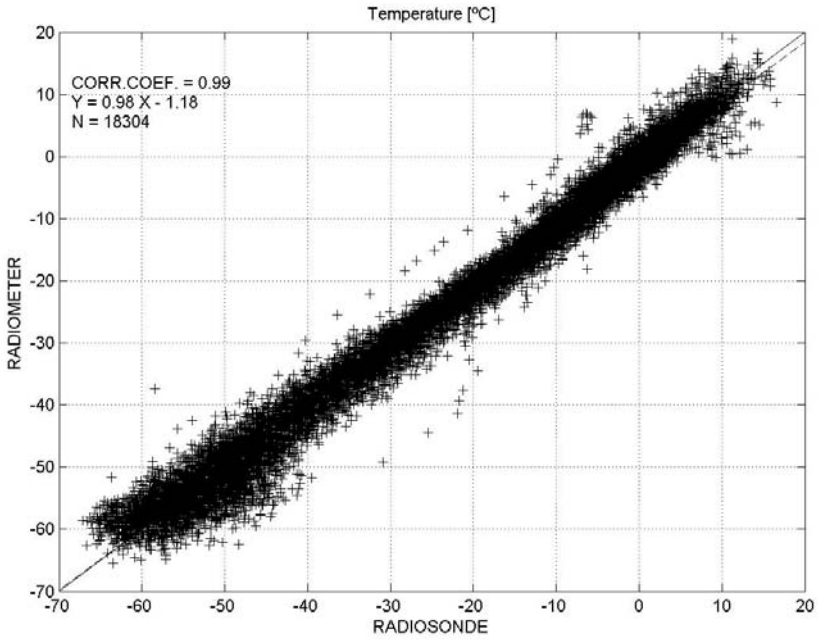

Figure 2: Comparison of radiometric and sounding temperature profiles using all the profiles at 0000 and 1200 UTC. The sample size, N , the correlation coefficient, (CORR.COEF), and the fitting are shown.

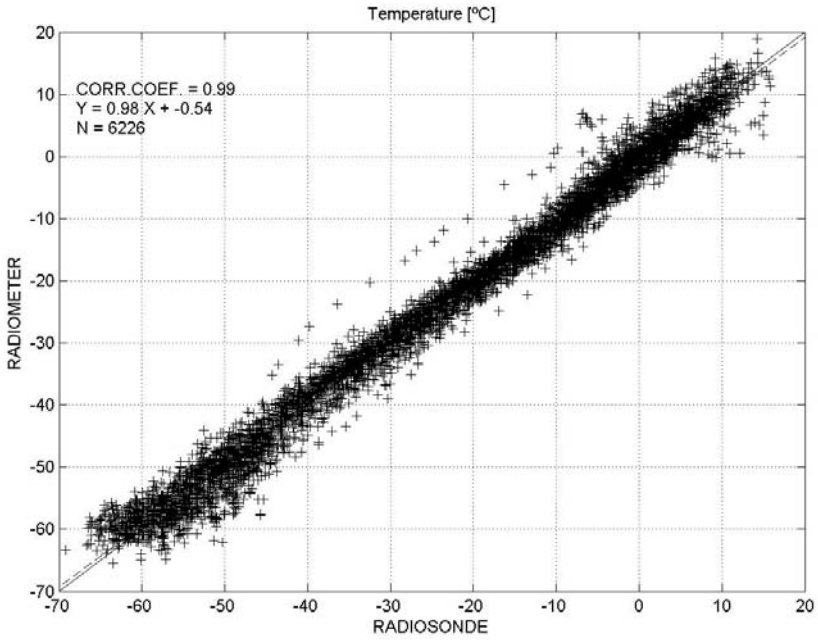

Figure 3: Comparison of radiometric and sounding temperature profiles using all the profiles when no precipitation was detected at 0000 and/or at 1200 UTC. The sample size, N, the correlation coefficient, (CORR.COEF), and the fitting are shown.

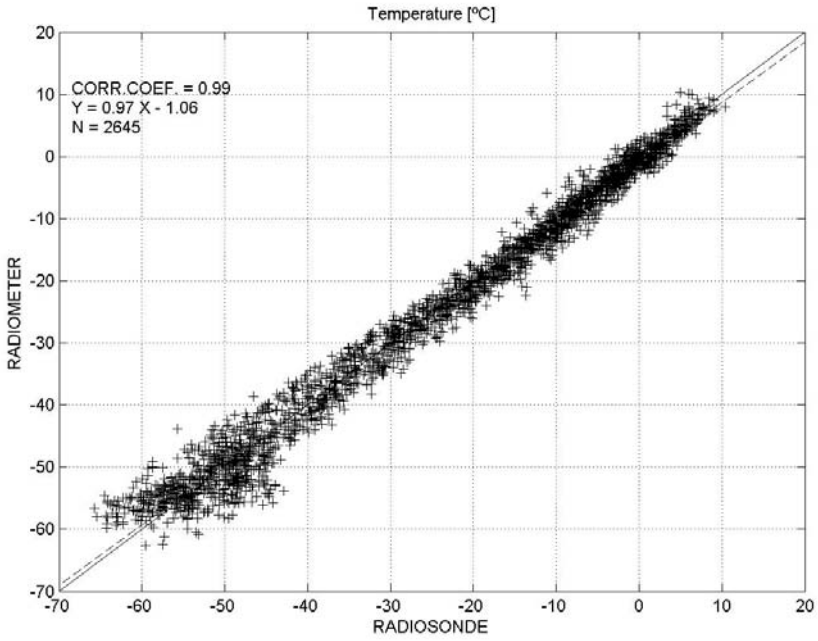

Figure 4: Comparison of radiometric and sounding temperature profiles using all the profiles when precipitation was detected at 0000 and/or at 1200 UTC. The sample size, N , the correlation coefficient, (CORR.COEF), and the fitting are shown.

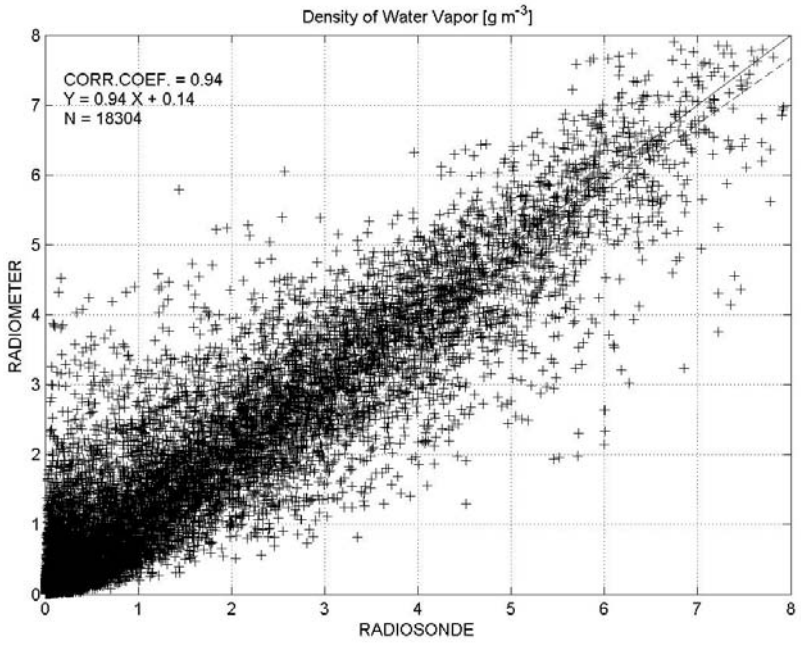

Figure 5: Comparison of radiometric and sounding profiles of water vapor density us- ing all the profiles at 0000 and 1200 UTC. The sample size, N, the correlation coefficient, (CORR.COEF), and the fitting are shown.

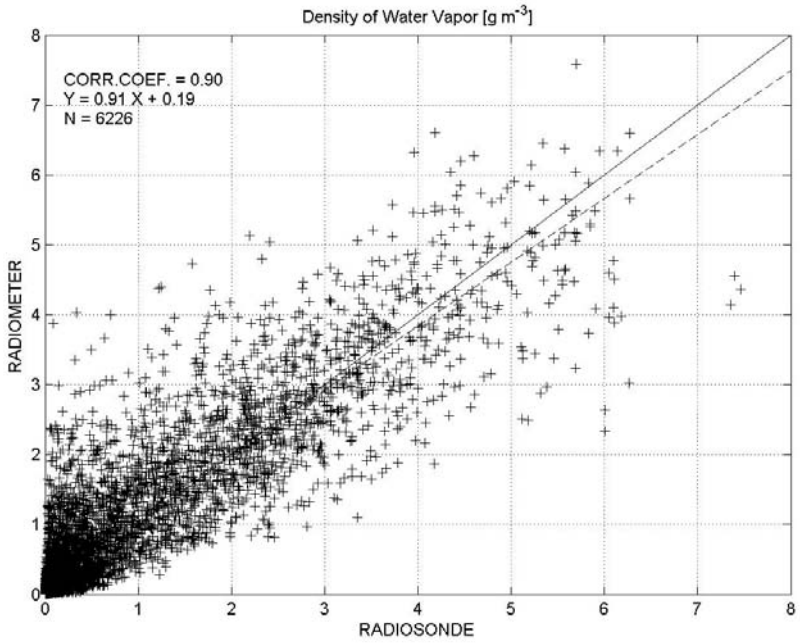

Figure 6: Comparison of radiometric and sounding profiles of water vapor density using all the profiles when no precipitation was detected at 0000 and/or at 1200 UTC. The sample size, N, the correlation coefficient, (CORR.COEF), and the fitting are shown.

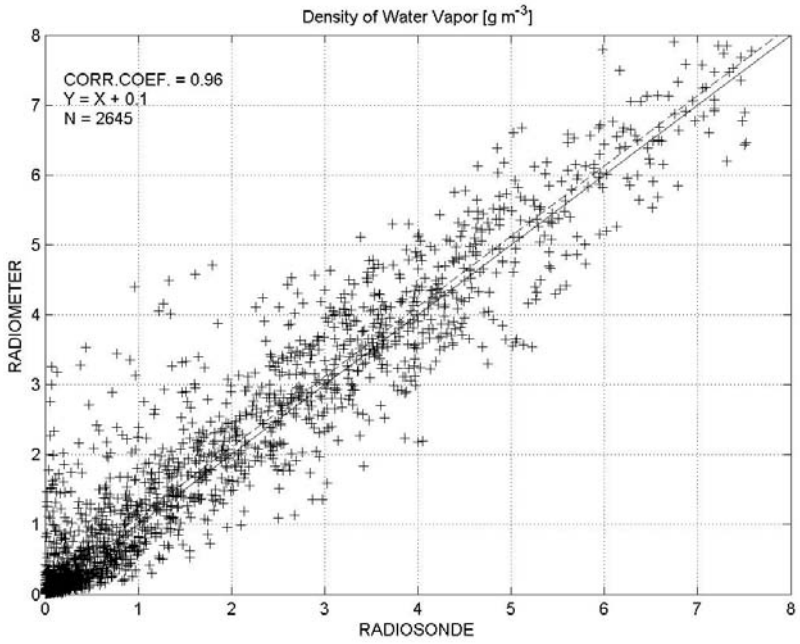

Figure 7: Comparison of radiometric and sounding profiles of water vapor density using all the profiles when precipitation was detected at 0000 and/or at 1200 UTC. The sample size, N, the correlation coefficient, (CORR.COEF), and the fitting are shown.

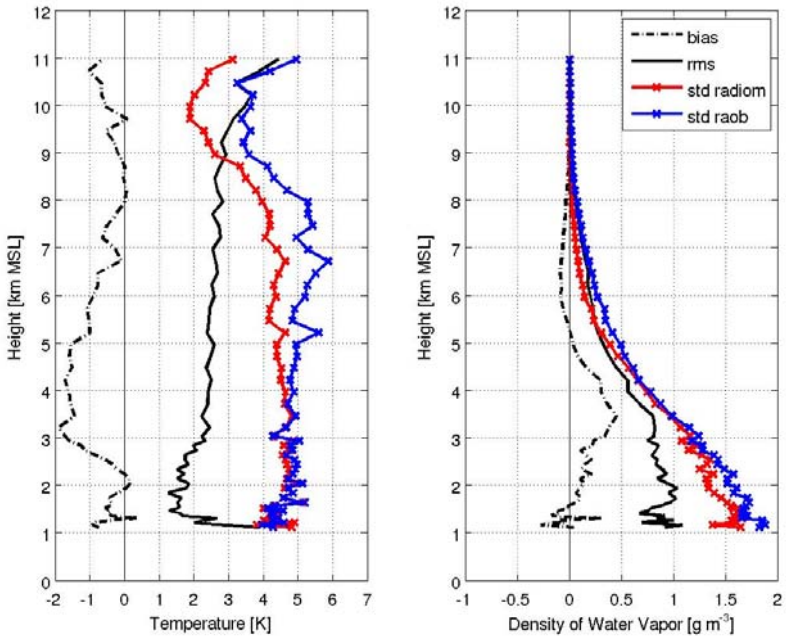

Figure 8: Retrieval error statistics for temperature (left) and density of water vapor (right), for all the profiles at 0000 and 1200 UTC. The bias, root mean square (rms), and standard deviation for the RAOB (std RAOB) in Madrid Barajas and for MMWR (std radiom) are shown.

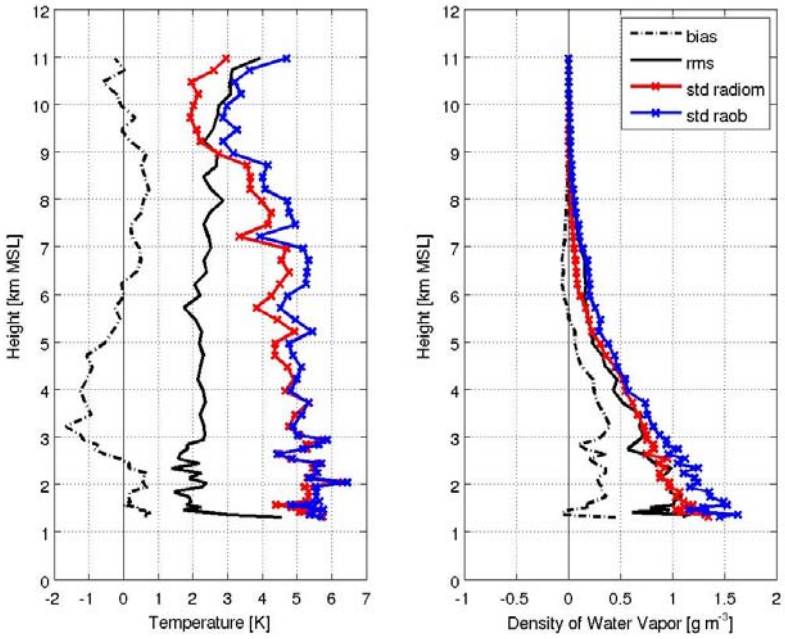

Figure 9: Retrieval error statistics for temperature (left) and density of water vapor (right), for the profiles when precipitation was not detected at 0000 and/or at 1200 UTC. The bias, root mean square (rms), and standard deviation for the RAOB (std RAOB) in Madrid Barajas and for MMWR (std radiom) are shown.

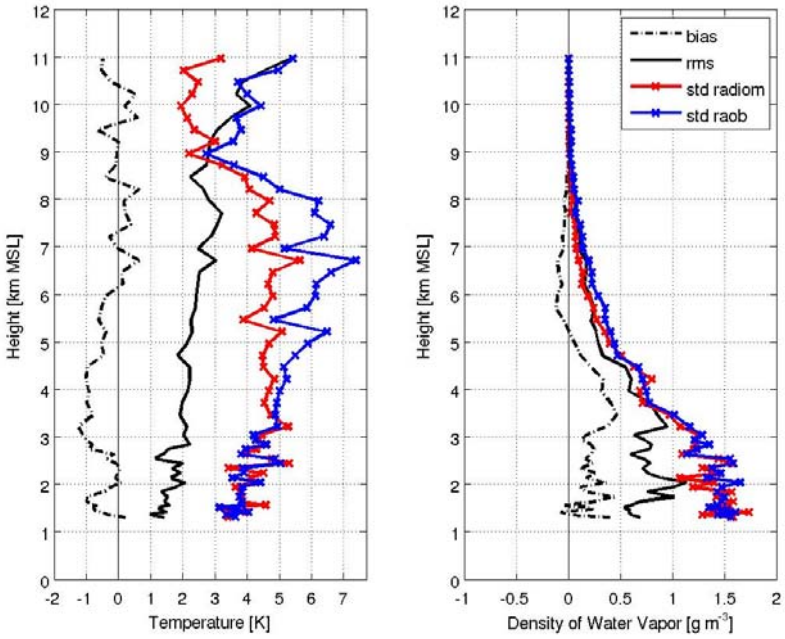

Figure 10: Retrieval error statistics for temperature (left) and density of water vapor (right), for the profiles when precipitation was detected at 0000 and/or at 1200 UTC. The bias, root mean square (rms), and standard deviation for the RAOB (stand RAOB) in Madrid Barajas and for MMWR (stand radiom) are shown.

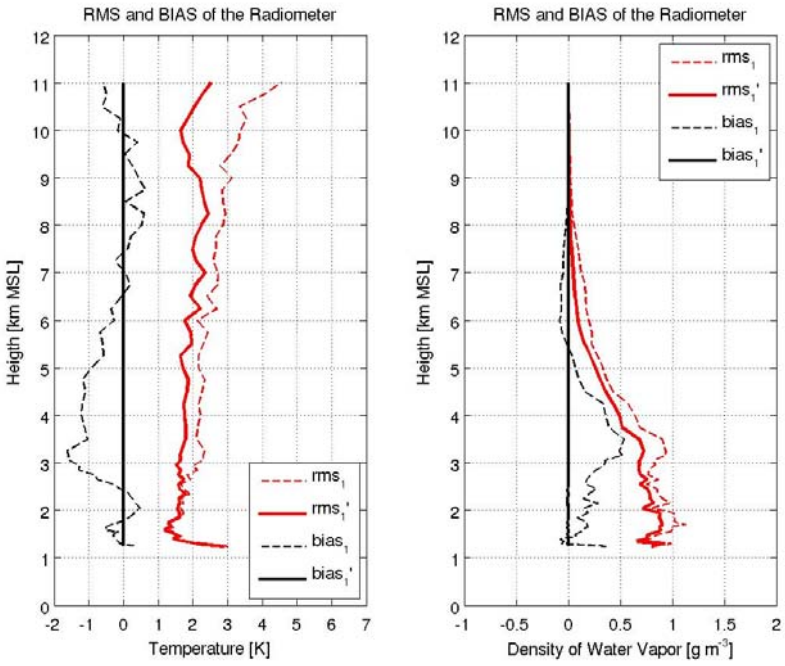

Figure 11: On the left: original (dashed lines) and corrected (bold lines) RMS and BIAS for retrieved temperature; and on the right for water vapor density. The bias and rms are shown for Sample 1 and Sample 2.

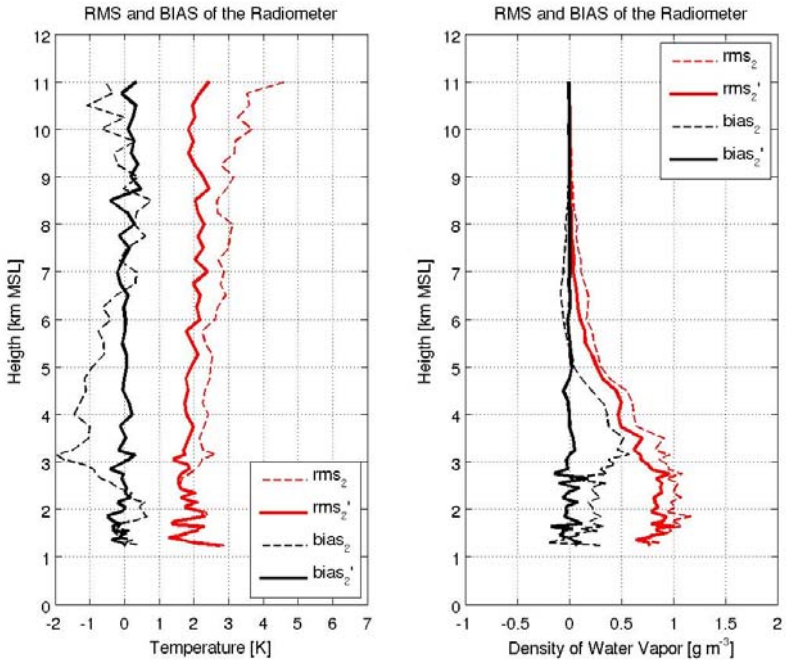

Figure 12: a) Original (dashed lines) and corrected (bold lines) RMS and BIAS for retrieved temperature; and b) same as Figure 11a but for water vapor density.